



ELSEVIER

Contents lists available at ScienceDirect

Biomaterials

journal homepage: www.elsevier.com/locate/biomaterials

Nanophotosensitizer-engineered *Salmonella* bacteria with hypoxia targeting and photothermal-assisted mutual bioaccumulation for solid tumor therapy

Fuming Chen^{a,b,1}, Zhongsheng Zang^{c,1}, Ze Chen^{a,1}, Liao Cui^b, Zhiguang Chang^c, Aiqing Ma^{a,b}, Ting Yin^a, Ruijing Liang^a, Yutong Han^{a,b}, Zhihao Wu^a, Mingbin Zheng^{a,b,***}, Chenli Liu^{c,**}, Lintao Cai^{a,*}

^a Guangdong Key Laboratory of Nanomedicine, CAS-HK Joint Lab for Biomaterials, CAS Key Lab for Health Informatics, Shenzhen Engineering Laboratory of Nanomedicine and Nanoformulations, Shenzhen Institutes of Advanced Technology (SIAT), Chinese Academy of Sciences, Shenzhen, 518055, PR China

^b Guangdong Key Laboratory for Research and Development of Natural Drugs, Key Laboratory for Nanomedicine, Guangdong Medical University, Dongguan, 523808, PR China

^c Institute of Synthetic Biology, Shenzhen Institutes of Advanced Technology, Chinese Academy of Sciences, 1068 Xueyuan Avenue, University Town, Nanshan, Shenzhen, 518055, PR China

ARTICLE INFO

Keywords:

Bacteria-driven nanophotosensitizer
Hypoxia-targeting
Tumor penetration
Mutual bioaccumulation
Photothermal therapy

ABSTRACT

Bacteria-driven drug-delivery systems have attracted great attention for their enhanced therapeutic specificity and efficacy in cancer treatment. YB1, a particularly attractive genetically modified safe *Salmonella Typhimurium* strain, is known to penetrate hypoxic tumor cores with its self-driven properties while remarkably avoiding damage to normal tissues. Herein, nanophotosensitizers (indocyanine green (ICG)-loaded nanoparticles, INPs) were covalently attached to the surface of YB1 with amide bonds to develop a biotic/abiotic cross-linked system (YB1-INPs) for tumor precision therapy. YB1 microswimmer retained its viability after efficiently linking with INPs. This YB1-INPs treatment strategy demonstrated specific hypoxia targeting to solid tumors, perfect photothermal conversion, and efficient fluorescence (FL) imaging properties. Benefited from the combined contribution of tumor tissue destruction and the bacteria-attracting nutrients generation after photothermal treatment, the bioaccumulation of YB1-INPs was significantly improved 14-fold compared to no photothermal intervention. Furthermore, YB1-INPs pervaded throughout the large solid tumor ($\geq 500 \text{ mm}^3$). Under near-infrared (NIR) laser irradiation, YB1-INPs exhibited a dependable and highly efficient photothermal killing ability for eradicating the large solid tumor without relapse. This strategy of bacteria-driven hypoxia-targeting delivery has a great value for large solid tumors therapy with low toxicity and high efficiency.

1. Introduction

Medicines are often taken to kill unwanted bacteria. However, a counter-intuitive approach—converting bacteria into medicine—has recently been gaining application [1,2]. Bacteria-mediated treatments have attracted significant attention, especially for tumor therapy due to the unique tumor colonizing ability of bacteria [3–5]. Various genetically modified bacterial strains have been constructed for cancer treatment. Such strains are characterized by high tumor accumulation and reduced toxicity and can deliver cytotoxic agents, cytokines,

angiogenesis inhibitors, antigens, and antibodies to disease sites, including tumors [6–9].

Salmonella Typhimurium YB1 (YB1), *Clostridium* and *Bifidobacterium* effectively targets tumor hypoxic cores as therapeutic vectors [10–13]. In YB1 (a genetically modified safe bacterial strain), the essential gene *asd* was replaced with a construct containing a gene that is controlled by hypoxia-targeted promoters. This substitution endowed YB1 microswimmer with an excellent hypoxia-targeting ability. Meanwhile, YB1 can penetrate tumors by detecting and chemotaxing towards nutrient [14,15]. This YB1 strain has been demonstrated to accumulate

* Corresponding author.

** Corresponding author.

*** Corresponding author. Guangdong Key Laboratory of Nanomedicine, CAS-HK Joint Lab for Biomaterials, CAS Key Lab for Health Informatics, Shenzhen Engineering Laboratory of Nanomedicine and Nanoformulations, Shenzhen Institutes of Advanced Technology (SIAT), Chinese Academy of Sciences, Shenzhen, 518055, PR China.

E-mail addresses: mb.zheng@siat.ac.cn (M. Zheng), cl.liu@siat.ac.cn (C. Liu), lt.cai@siat.ac.cn (L. Cai).

¹ These authors contributed equally to this work.

up to 1000 times more in tumors than in other organs [16]. YB1 was also proven to reduce the risk of septic shock in the host [16]. However, YB1 is still limited in cancer therapy, especially for large solid tumors ($\geq 500 \text{ mm}^3$ in volume) due to unsatisfactory therapeutic efficiency and easy recurrence [17–19]. The reason is that anaerobes can selectively colonize and destroy hypoxic regions but leave a well-oxygenated outer rim of the large solid tumors that can lead to tumor recurrence [20–22].

The combination of nanotechnology and biological carriers has been demonstrated as a promising strategy for overcoming delivery through physiological barriers (tumor hypoxic barrier, blood–brain barrier, tissue penetration barrier, etc.) and achieving enhanced antitumor effectiveness [23,24]. One example is the *Magnetococcus marinus* strain MC-1. MC-1 bacteria rely on geomagnetic-assisted aerotaxis (known as magneto-aerotaxis) to efficiently deliver drug-containing nanoliposomes to the oxic–anoxic transition zone (OATZ) [25]. As endogenous cells, neutrophils carrying liposomes that contain paclitaxel can penetrate the brain and suppress the recurrence of glioma in mice whose tumor has been resected surgically [26]. However, both of these strategies have intrinsic drawbacks. Chemotherapy drugs inevitably produce potential toxic side effects to biological carriers. Previously, we developed indocyanine green (ICG)-loaded nanoparticles (INPs) as a nanophotosensitizer for fluorescence-guided photothermal therapy (PTT) of tumors. Compared with widely used photothermal agents [27–34], INPs are of particular interest because they have good biocompatibility, and exhibit high spatiotemporal selectivity or excellent photothermal conversion efficiency [35,36]. By combining the advantages of nanophotosensitizers and microbes, INPs can potentially overcome the shortcomings of low tumor inhibition by native bacteria and effectively reduce the therapeutic dosage of nanodrugs. With the potential to benefit from the mutual advantages of both nanophotosensitizers and microbes, this combination could achieve safer and more effective treatment of large solid tumors.

Here, we developed a biotic/abiotic cross-linked system (YB1-INPs) for large solid tumor precision therapy (Fig. 1). The YB1-INPs maintained the viability of YB1 microswimmers and the theranostics properties of INPs, after INPs were covalently linked on the surface of YB1. We sought to harness the hypoxia-targeting ability of YB1 to deliver the

biocompatible photothermal agent (INPs) to hypoxic tumor cores, which facilitated the effective tumor accumulation of INPs. Afterwards, the photothermal effects of INPs could kill tumor cells and loosen the tumor tissue, resulting in attracting abundant YB1-INPs and promoting YB1-INPs infiltration throughout the whole tumor. Finally, under near-infrared (NIR) laser irradiation, the temperature up to 63°C in the tumor area, so that both the tumors and intratumoral YB1 were eradicated simultaneously to achieve a high efficiency photothermal therapy. This work presents a bacteria-mediated hypoxia-targeting strategy for the diagnosis and eradication of deep-seated or advanced solid tumors.

2. Materials and methods

2.1. Materials

ICG, PLGA (lactide, glycolide (50:50); MW, 5000–15000), and hematopylin and eosin (H&E) were purchased from Sigma–Aldrich (USA). Soybean lecithin and distearoylphosphatidylethanolamine derivatives of PEG with a terminal carboxyl group (DSPE-PEG2000-COOH) were obtained from Avanti (USA). Cholesterol, N-hydroxysulfosuccinimide (sulfo-NHS), 1-ethyl-3-[3-(dimethylamino) propyl]-carbodiimide (EDC), 2-(N-morpholino)-ethanesulfonic acid (MES), Sepharose CL-4B, glutaraldehyde and phosphate-buffered saline (PBS) were all acquired from Sigma–Aldrich (USA). Hoechst 33258 was purchased from Invitrogen (USA). Penicillin–streptomycin, fetal bovine serum, Luria Broth (LB) medium, Dulbecco's modified Eagle's medium (DMEM)/F12 medium, and trypsin ethylenediaminetetraacetic acid (EDTA) were acquired from Gibco Life Technologies (USA). The LIVE/DEAD BacLight bacterial viability kit was obtained from Invitrogen (USA). Amicon ultra-4 centrifugal filters with a molecular weight cutoff of 10 kDa were purchased from Millipore (USA). Sterile 6.5-mm Transwell® plates with 3.0- μm pore polycarbonate membrane inserts were obtained from Corning (USA). The KIT-9710 UltraSensitive™ S-P Hypersensitivity Kit (rat/rabbit) and DAB-2031 enhanced DAB chromogenic kit were provided by MXB (CHN). Anti-Salmonella antibody and goat anti-rabbit IgG H&L (Alexa Fluor® 594) were obtained from

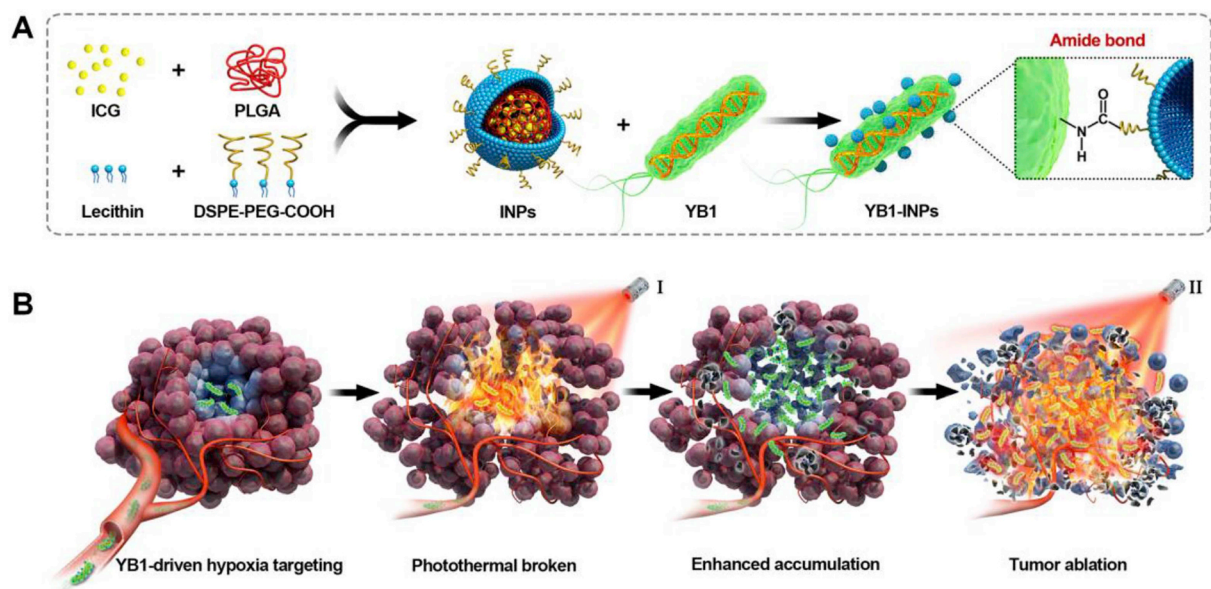


Fig. 1. Schematic illustration of nanophotosensitizers (INPs)-attached YB1 as a hypoxia-targeting delivery system for large solid tumors photothermal therapy. A) Preparation procedure of YB1-INPs. Synthesized INPs with single-step sonication were attached to YB1 through amide bonds. B) YB1-INPs with hypoxia-targeting and photothermal-assisted bioaccumulation for tumor penetrative therapy. After migrating into tumor hypoxic cores and subsequently irradiating with NIR laser, the loosening of tumor tissue and tumor lysis generate bacteria-attracting nutrients, which further enhances the accumulation and coverage of YB1-INPs in large solid tumors. Ultimately, the enriched YB1-INPs under NIR laser irradiation completely ablated the large solid tumor without relapse.

Abcam (U.K.). The Hypoxyprobe™-1 Plus Kit was purchased from Hypoxyprobe, Inc (USA). The liver or renal function activity assay kit was obtained from Jian Cheng Biotech (CHN). Glucose, glucose oxidase, and catalase were acquired from Aladdin (CHN).

2.2. Formulation of INPs

INPs were synthesized from PLGA, soybean lecithin, ICG, and DSPE-PEG-COOH using a previously reported single-step sonication method [36]. PLGA was dissolved in 80% acetonitrile aqueous solution at a concentration of 2 mg/mL. To generate INPs, (lecithin)/(DSPE-PEG-COOH) (mass ratio was 2:3) with a total mass ratio of 15% to PLGA polymer and 750 µg of ICG were added in 3 mL of 4%-ethanol aqueous solution, and the PLGA solution was added dropwise under sonication using an ultrasonics processor (VCX130, USA) at a frequency of 20 kHz and a power of 130 W for 5 min. Finally, the INPs were washed three times using an Amicon ultra-4 centrifugal filter.

2.3. Characterization of the INPs

The morphology of the INPs was characterized by TEM (FEI Tecnai G2 F20 S-Twin, USA). The size distribution of the INPs was measured by a Zetasizer Nano ZS (Malvern, U.K.). The UV-vis absorption spectra of the INPs and YB1-INPs were measured by UV/vis spectrometry (Lambda25, Perkin-Elmer, USA) in dimethyl sulfoxide (DMSO). The fluorescence spectra of the INPs and YB1-INPs were obtained by fluorescence spectroscopy with excitation at 808 nm (F900, Edinburgh Instruments, Ltd., U.K.) in dimethyl sulfoxide (DMSO). Quartz cuvettes with the INPs, free ICG and PBS were treated with 1 W/cm² 808-nm laser irradiation (Leimai, China) for 10 min. Infrared thermographic maps were obtained by an infrared thermal imaging camera (Fluke Ti27, USA).

2.4. Salmonella YB1 and tumor cells culture

S. typhimurium strain YB1 was kindly provided by Dr. Jiandong Huang. YB1 was inoculated into a tube containing LB broth supplied with 25 µg/mL chloramphenicol and cultured at 37 °C with shaking at 220 rpm overnight. The YB1 cultures were then transferred twice and grown to logarithmic phase. Finally, YB1 was suspended in PBS buffer for internal and external experiments.

The MB49 mouse bladder cancer cell line was maintained in DMEM supplemented with 10% heat-inactivated fetal bovine serum, 1% streptomycin and 1% penicillin. Cells were cultivated at 37 °C in a humidified atmosphere of 5% CO₂.

2.5. Covalent coupling of carboxylated INPs to YB1 using carbodiimide chemistry

To stably couple INPs to the surface of YB1 bacteria, we exploited the fact that cells have high levels of intrinsic amine groups on their surfaces [25]. The most straightforward approach to immobilize and maintain functionalized INPs with reactive carboxylic acid groups (-COOH) to the surface amine groups (-NH₂) of bacteria is to use direct covalent chemical conjugation [37].

First, 1 mL of INP solution (400 µg/mL) were activated by incubation with the EDC and sulfo-NHS (EDC/NHS/DSPE-PEG-COOH molar ratio were 30:30:3) for 40 min in 3 mL MES buffer (pH = 5.5) at room temperature. A dialysis bag (MW:3500) was used to remove the excess reagents. Subsequently, bioconjugation was achieved by incubating approximately 10⁸ CFU of YB1 with activated INPs in PBS. The mixture was then incubated for 2 h at 37 °C under gentle agitation to permit amide coupling. YB1-INPs were separated from unbound INPs using 3500 rotation centrifugation followed by three rinses with PBS. The sample was resuspended in PBS at pH 7.4.

2.6. Assessment of nanoparticle attachment to YB1 microswimmers

The morphology of YB1 and YB1-INPs was characterized by SEM (VEGA 3 SBH, Czech Republic). Detailed SEM samples were prepared as follows. First, YB1-INPs were fixed with 4% glutaraldehyde in 0.5 mL of PBS (pH 7.2) at 4 °C. Fixed samples (50 µL) were placed onto silicon slices and then rinsed with ultrapure water. Next, the samples were dehydrated in a series of ethanol/water solutions with increasing ethanol content from 30% to 100%. The ethanol was displaced in a series of tert-butyl alcohol/water solutions of increasing tert-butyl alcohol content from 40% to 100%. Finally, the tert-butyl alcohol in the sample was removed by freeze-drying [25].

YB1-INPs (200 µL of PBS, 1 × 10⁷/well) were added in eight-well chambered coverglasses (Lab-Tek, Nunc, USA). Images were observed through a 63.0 × 1.4 oil-immersion objective, and FL signals from YB1-INPs were acquired using TCS SP5 confocal laser scanning microscopy (TCS SP5II, Leica, Ernst-Leitz-Strasse, Germany).

The size distributions of the INPs, YB1 and YB1-INPs were detected by a Zetasizer Nano ZS (Malvern, U.K.). The absorption spectra of the INPs and YB1-INPs were evaluated by UV/vis spectrometry (Lambda25, Perkin-Elmer, USA), and the FL spectra of the INPs and YB1-INPs were evaluated using FL spectroscopy with excitation at 740 nm (F900, Edinburgh Instruments, Ltd., U.K.). The ICG concentrations of the INPs and YB1-INPs were quantified by measuring the FL intensity at 808 nm.

2.7. Bacterial viability assay

The effect of the INPs on the viability of YB1 was evaluated using a LIVE/DEAD BacLight bacterial viability kit (Invitrogen, USA) according to the manufacturer's protocol [38]. The assay kit included green FL SYTO 9 dye to mark viable bacteria and propidium iodide (PI) dye to detect dead bacteria. Live YB1 was stained green, and dead YB1 was stained red with PI. The stained bacterial suspension was placed between a slide and an 18-mm² coverslip for examination by FL microscopy.

To further evaluate the safety of INPs, YB1 and YB1-INPs containing equal amounts of YB1 at 10 × dilution (three repeated trials) were cultured on solid LB agar (Gibco Life Technologies, USA) for 24 h, and bacterial growth was observed by counting the bacterial colonies [39].

2.8. Chemotaxis machinery of YB1-INPs microswimmers

The chemotaxis of YB1-INPs was investigated using a Transwell migration assay (Transwell polycarbonate membrane: 3 µm pore size, 6.5 mm diameter and 0.33 cm² membrane surface area) (Corning, USA).

For hypoxia simulation, YB1-INPs (200 µL, 5 × 10⁷ CFU/mL) were added to the upper chamber, and 0.4 mL of glucose solution (0.4 mg/mL), glucose oxidase (0.5 KU) and catalase (0.5 KU) were added to the bottom chamber. We utilized glucose and glucose oxidase reactions to simulate hypoxia. We utilized catalase to eliminate the hydrogen peroxide produced by the above reaction. For the control group, the bottom chamber was filled with 0.4 mL of glucose solution. The YB1-INPs in the bottom and upper chamber were collected for DAPI (4',6-diamidino-2-phenylindole) staining at various time points. Afterwards, the quantity of bacteria in the bottom and upper chamber was detected by flow cytometry. To more intuitively observe the migration of YB1-INPs microswimmers, the contents of the bottom chamber were transferred to eight-well chambered coverglasses (Lab-Tek, Nunc, USA) after a 40 min migration period. FL signals from the YB1-INPs were acquired using TCS SP5 confocal laser scanning microscopy (TCS SP5II, Leica, Ernst-Leitz-Strasse, Germany).

For nutrition simulation, YB1-INPs (200 µL, 5 × 10⁷ CFU/mL) and MB49 cells (200 µL of PBS, 1 × 10⁵ cells) were added to the upper and bottom chambers, respectively. The bottom chamber was then filled with 0.2 mL of INPs solution (35 µg/mL) and treated with NIR laser

irradiation (808 nm, 1 W/cm², 5 min) to kill the MB49 cells. Bacterium-attracting nutrients generated by cell death induced the migration of the YB1-INPs. The quantity of YB1-INPs in the bottom chamber was counted via an LB agar plate assay at various time points. After a 40-min migration period, the YB1-INPs in the bottom chamber were separated from free INPs by centrifugation at 3500 rpm followed by three rinses with PBS. Subsequently, the sample was added to eight-well chambered coverglasses for confocal imaging.

2.9. Animals and tumor model

Animals received care in accordance with the Guidance Suggestions for the Care and Use of Laboratory Animals. The procedures were approved by the Animal Care and Use Committee (Shenzhen Institutes of Advanced Technology, Chinese Academy of Sciences). Four-to six-week-old female C57 BL/6 mice (Vital River Laboratory Animal Technology Co. Ltd, CHN) were subcutaneously injected with MB49 cells (1×10^6) in the flank region. Tumor volume was calculated according to the following formula: tumor volume = length \times (width)²/2.

2.10. In vivo imaging and biodistribution analysis

When the volumes of the MB49 tumors reached about 500 mm³, the C57BL/6 mice were randomly divided into three groups and injected with INPs or YB1-INPs (125 μ L, 56 μ g/mL INPs) via the tail vein. A 125- μ L volume of YB1-INPs contained 10^7 YB1. The YB1-INPs (+) group was treated with NIR laser irradiation at 12 h after intravenous injection of YB1-INPs. The FL signals of ICG were obtained by an *ex/in vivo* imaging system (CRi Maestro, USA) (ex: 704 nm and filter: 735 nm). The mice were killed 72 h after injection. The major organs (heart, liver, spleen, lung, kidneys) and tumors were collected for semi-quantitative biodistribution analysis and imaging using the *ex/in vivo* imaging system (CRi Maestro, USA).

The FL signal from tissue and plasma samples treated with ICG were > 20 times higher than the signal from non-treated samples (*i.e.* background), FL spectrometry was successfully used for *in vivo* quantification of ICG [40]. To extract ICG, the urine/feces of C57BL/6 mice were homogenized in 5 mL of dimethyl sulfoxide (DMSO), and centrifuged at 9000 rpm for 15 min. The ICG content of each sample was determined by FL spectrometry. Blood samples were centrifuged at 16000 g for 5 min, and the plasma was utilized for evaluation of blood circulation time curve.

2.11. Immunohistochemical staining

Tumor-bearing mice were intravenously (*i.v.*) injected with INPs and YB1-INPs at an INPs dose of 0.35 mg/kg. The tumors were embedded in optimal cutting temperature compound (OTC) and sectioned 72 h after injection (Leica, Germany). To detect YB1, tumor sections were incubated with a KIT-9710 UltraSensitive™ S-P Hypersensitivity Kit (rat/rabbit, MXB, CHN) to stain YB1. After staining nuclei with DAPI, the slices were observed by an FL optical microscope [24].

2.12. Immunofluorescence staining

To better visualize the hypoxic tumor regions and to demonstrate colocalization of YB1, tumor-bearing mice were *i.v.* injected with INPs and YB1-INPs at an INPs dose of 0.35 mg/kg, respectively. The YB1-INPs (+) group were treated with NIR laser irradiation at 12 h after intravenous injection of YB1-INPs. At 72 h post-injection, the mice were intraperitoneally injected with pimonidazole hydrochloride (60 mg/kg) (Hypoxyprobe™-1 Plus Kit) [41]. One hour later, the tumors were harvested from the various groups, sectioned and incubated with FITC-Mab1 (dilution 1:100) (Hypoxyprobe™-1 Plus Kit) and polyclonal rabbit anti-YB1 receptor (dilution 1/100 for 2 h at room temperature) antibodies. The slides were then incubated with goat anti-rabbit IgG H&

L (Alexa Fluor® 594) to visualize YB1 receptors based on purple color development (dilution 1/100 for 1 h at room temperature).

After staining with DAPI, the slices were observed by an Invitrogen EVOS FL Auto 2 system (Thermo Fisher Scientific, CHN). Immunofluorescence images of tumor sections were analyzed using Celleste™ and converted to corresponding surface plot images [42]. To explore the hypoxic targeting capability and the photothermal-assisted bioaccumulation efficiency of the YB1-INPs, the fluorescent data at the arrow in the surface plot images were further extracted for semi-quantitative analysis.

2.13. Temperature measurement during laser irradiation

C57BL/6 mice bearing MB49 tumors were injected *i.v.* with INPs or YB1-INPs (56 μ g/mL INPs, 125 μ L), and control mice were treated with 125 μ L of PBS. At 72 h, the tumors were irradiated with a laser (808 nm, 1 W/cm²) for 5 min. The regional maximum temperatures and infrared thermographic maps were obtained by a Ti27 infrared thermal imaging camera (Fluke, USA).

2.14. Temperature tolerance analysis of YB1

YB1-INPs (1 mL, 6×10^6 CFU/mL) were added to quartz cuvettes and treated with NIR laser irradiation (808 nm, 1 W/cm²). The number of live bacteria were counted via an LB agar plate assay with increasing temperature.

2.15. Antitumor effect and biosafety of biohybrid microswimmers (YB1-INPs) in vivo

C57BL/6 mice (5 per group) bearing large solid tumors (≥ 500 mm³ in volume) were injected with YB1-INPs (125 μ L, containing 56 μ g/mL INPs and 10^7 CFU of YB1), INPs (125 μ L, 56 μ g/mL INPs) and PBS (125 μ L) via the tail vein [18,19]. At 12 h post-injection, the first dose of laser irradiation (808 nm, 1 W/cm², 5 min) was used to kill tumor cells to produce bacteria-attracting nutrients and further damage the tumor tissue, resulting in the recruitment of more YB1-INPs and promoting YB1-INP infiltration. At 72 h post-injection, the second laser dose (808 nm, 1 W/cm²) was used to irradiate the tumors for 5 min. One group of mice with YB1-INPs was not irradiated with the laser. The body weights of the mice and tumor volumes were monitored every 2 days. The appearance of the mice was photographed every 2 days with a Nikon camera (JPN). According to the animal protocol, the mice were assumed to be death when tumor size over 3000 mm³. To evaluate necrosis in tumor cell, representative tumors from each group of animals were collected, and stained with H&E at day 3.

C57BL/6 mice were injected with YB1-INPs and PBS via the tail vein. At 28 days post-treatment, ALT/ALP or UREA/CRE was evaluated using a liver or renal function activity assay kit (Jian Cheng Biotech, CHN). Major organs were excised and cut into 8- μ m sections for H&E staining, and sections were observed using an Olympus microscope (Olympus BX53, JPN).

3. Results and discussion

3.1. Preparation and characterization of YB1-INPs microswimmers

The fabrication process of YB1-INPs is described in Fig. 1A. First, nanophotosensitizers with carboxy groups in the shell (INPs) were self-assembled from ICG, poly (lactic-co-glycolic acid) (PLGA), soybean lecithin, and PEGylated phospholipid (DSPE-PEG-COOH) through a single-step sonication method [36]. Then, terminal amine groups on the outer membrane of bacteria and carboxy groups of INPs with amide bonds were conjugated using 1-ethyl-3-[3-(dimethylamino)propyl]-carbodiimide/N-hydroxysulfosuccinimide (EDC/NHS) crosslinking, forming biohybrid microswimmers (YB1-INPs). Representative scanning electron microscopy (SEM) images showed that over 60 INPs were

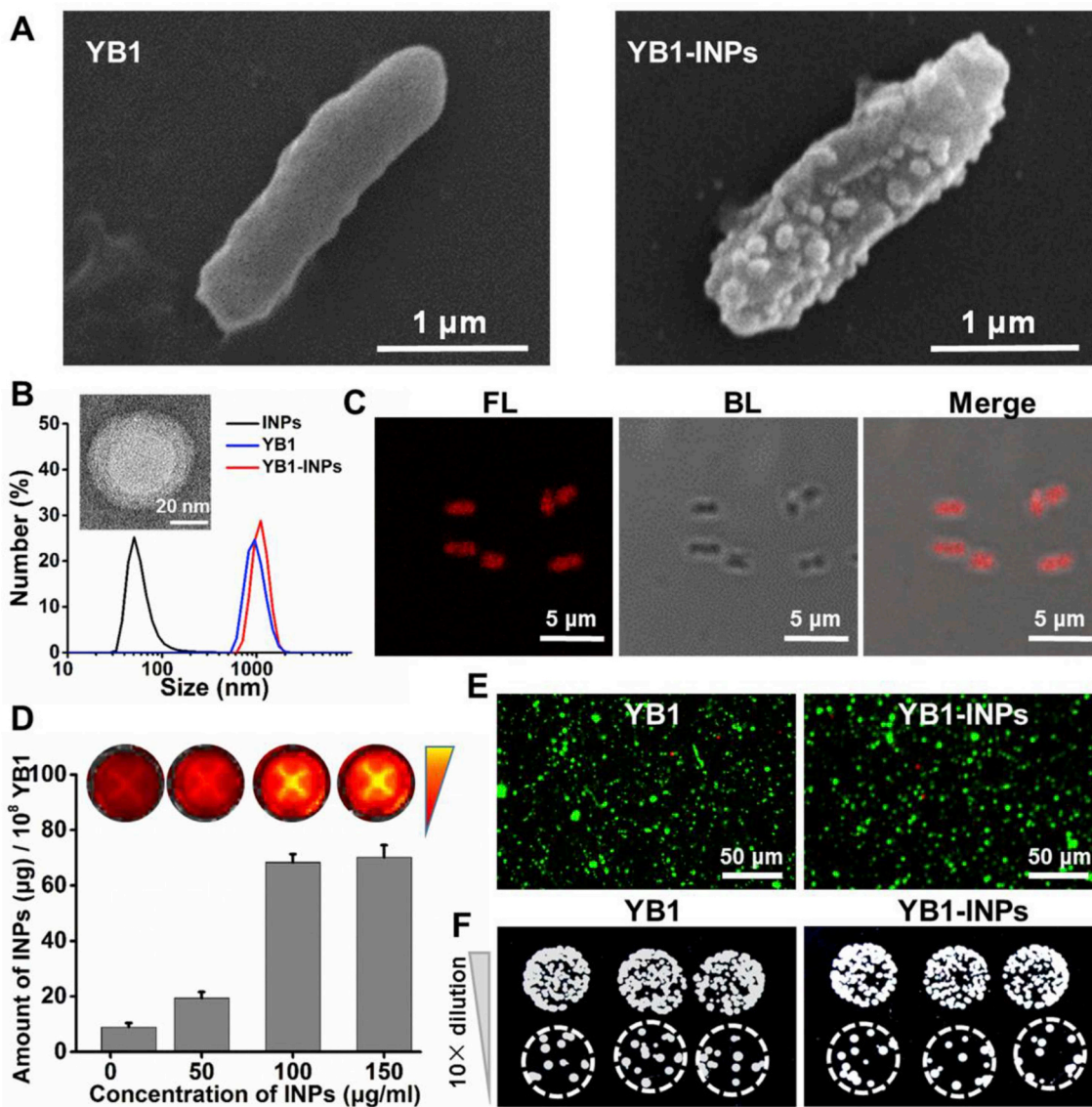


Fig. 2. Characterization of biohybrid microswimmers (YB1-INPs). A) SEM images of YB1 and YB1-INPs. B) Size distribution of INPs, YB1 and YB1-INPs. Inset: TEM image of INPs. C) Confocal microscopic images of ICG-labeled (red FL) YB1-INPs. D) INP weights attached to 10^8 CFU YB1. Inset: ICG FL images of the corresponding YB1-INP solutions. E) FL microscopic images of YB1-INPs. Live YB1 was stained green with SYTO 9, and dead YB1 was stained red with PI. F) Growth of YB1 and YB1-INPs was evaluated on solid LB agar. (Three independent experiments were performed.). (For interpretation of the references to color in this figure legend, the reader is referred to the Web version of this article.)

attached to the surface of each YB1 (Fig. 2A). Dynamic light scattering measurements revealed that the hydrodynamic sizes of YB1-INPs were slightly larger than YB1 due to the efficient attachment of INPs (approximately 50 nm) to the surface of YB1 (Fig. 2B). Infrared thermographic images of INPs indicated that INPs have excellent photothermal conversion efficiency as ICG (Fig. S1). Compared with INPs, the UV-vis spectra of YB1-INPs showed strong absorption peaks at 780 nm, the same as the absorption characteristic of INPs. Moreover, the fluorescent emission peak of YB1-INPs at 815 nm was consistent with that of INPs (Fig. S2). Fluorescence (FL) imaging results indicated that INPs, even after washing 3 times, still resided on the surface of YB1, allow real-time tracking of biohybrid microswimmers (YB1-INPs) (Fig. 2C). We next sought to improve the conjugation efficiency of INPs on the surface of YB1, YB1 was incubated with different concentrations of INPs for 2 h. We found that the amount of INPs anchoring was concentration-dependent. When the concentration of INPs was 100 $\mu\text{g/ml}$, the conjugation efficiency (10^8 CFU YB1) reached saturation. Thus, we chose INPs with a concentration of 100 $\mu\text{g/ml}$ for all further experiments and

analyses (Fig. 2D). Additionally, to investigate whether INPs conjugation affects the viability of YB1, live YB1 was stained green with SYTO 9, and dead YB1 was stained red with propidium iodide (PI) [38]. We found that conjugation of INPs with YB1 did not affect the viability of YB1 microswimmers (Fig. 2E). To further evaluate the safety of INPs, YB1 and YB1-INPs containing equal amounts of YB1 at $10 \times$ dilution (three repeated trials) were cultured on solid Luria broth (LB) agar for 24 h, and bacterial growth was observed by counting the bacterial colonies. The results in Fig. 2F revealed that the number of bacteria colonies formed by YB1 and YB1-INPs were similar, which indicated that the INPs material and conjugation process were safe to YB1.

3.2. Evaluation of hypoxia/nutritional migration of YB1-INPs microswimmers

To determine efficient hypoxia-targeting of YB1-INPs and the corresponding hypothesis of synergistic phototherapy, the well-established hypoxia/nutritional simulation was employed as an *in vitro* model

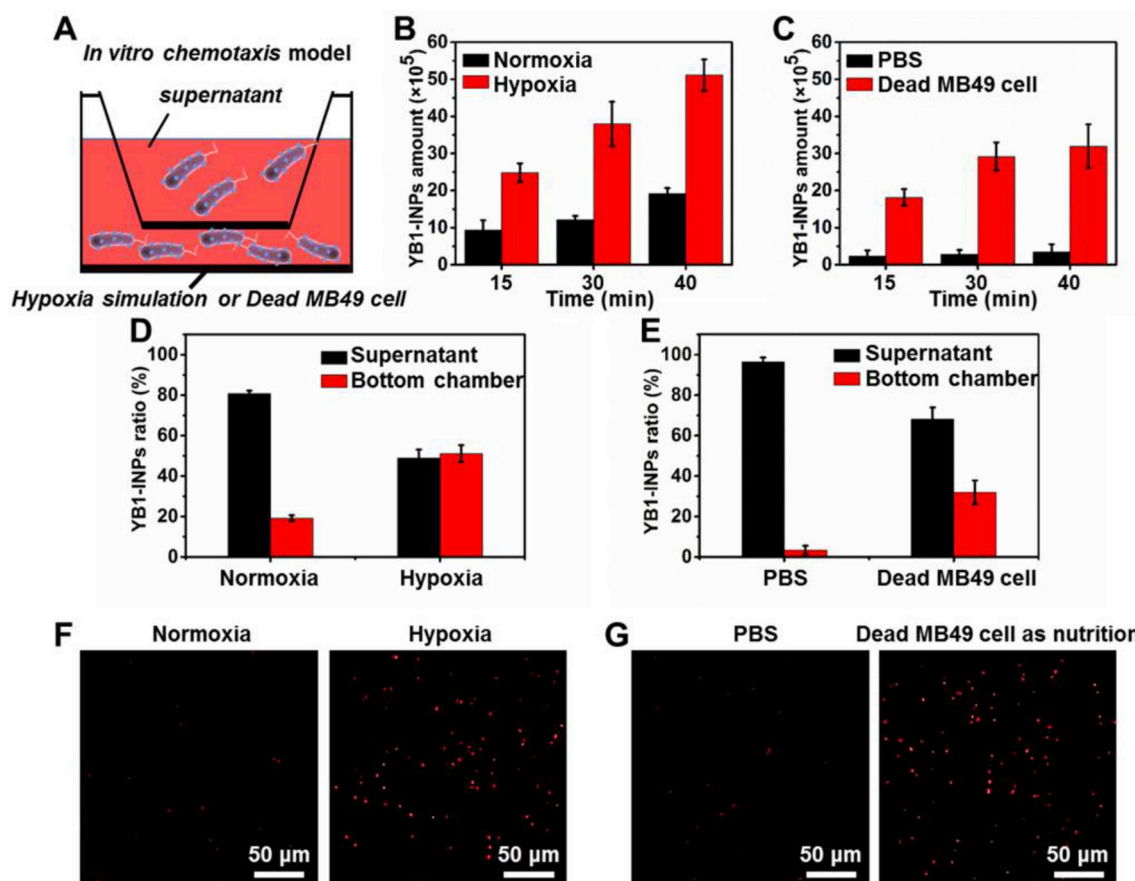


Fig. 3. Evaluation of the migration of YB1-INPs microswimmers in hypoxic or nutritional environments. A) Schematic illustration of the hypoxia and nutritional simulation model using a transwell system to evaluate the chemotaxis of YB1-INPs. B, C) YB1-INPs migration to the bottom chamber in the hypoxia-induced B) and nutrition (dead MB49 cells after photothermal therapy)-induced C) environments. The cells were counted by flow cytometry and LB agar plate assay. D, E) Percentage of migrated YB1-INPs after 40 min of incubation in hypoxic D) and nutritive E) solutions. F, G) FL imaging of hypoxia-induced F) and nutrition-induced G) migration of YB1-INPs to the bottom chamber.

[26,43]. In the hypoxia simulation model, the solution of the mixture including glucose, glucose oxidase and catalase were placed in the bottom of the chamber to construct a hypoxic microenvironment. Bacteria cultured in inserts were separated from the bottom chamber by polycarbonate membranes with a pore size of 3 μm . To explore the migration of YB1 under hypoxia induction, the quantity of YB1 with ICG-loaded nanoparticles in the bottom chamber was detected by flow cytometry at various points in time (Fig. 3B). We found that the tested YB1-INPs showed extremely low migration through the polycarbonate membrane under normoxic conditions. The quantity of YB1-INPs in the bottom chamber was only 19% after a 40-min migration period. In contrast, the quantity of YB1-INPs in the bottom chamber dramatically increased to 51% under hypoxic conditions (Fig. 3D). Notably, significant enhancement in the FL intensity could be observed after 40 min of migration, further indicating that a hypoxic environment can induce the migration of YB1-INPs to tumors (Fig. 3F).

MB49 cells in the bottom chamber were killed to generate bacteria-attracting nutrients by the INPs + laser, revealing the nutritive chemotaxis of YB1-INPs. As expected, the nutrients generated by cell death dramatically induced the migration of YB1-INPs according to quantitative analysis of flow cytometry and confocal laser scanning microscopy (CLSM) compared with the control group (PBS) (Fig. 3C and G). Finally, 32% of the total YB1-INPs migrated to the bottom chamber under nutrient condition, while only 4% migrated to the bottom chamber in the control group (Fig. 3E). Taken together, these results suggest that YB1-INPs as bacteria-driven microswimmers have the characteristics of hypoxia targeting and nutrition chemotaxis.

3.3. *In vivo* imaging and biodistribution analysis

Although the hypoxic microenvironment of large solid tumors is a barrier for many therapies, it is an ideal environment for a number of anaerobic bacteria [44,45]. We thus harnessed the tumor-targeting ability of YB1 to deliver INPs to hypoxic tumor areas. To explore the biodistribution of YB1-INPs, C57BL/6 mice bearing a transplanted MB49 tumor were intravenously injected with INPs or YB1-INPs. At 12 h postinjection, subgroups of mice were treated with or without laser irradiation. We then used an *in vivo* imaging system to monitor ICG FL in the animals over 72 h. There were obvious differences in the FL distribution among the samples. No obvious FL signals were detected in the INPs group because of the lack of active targeting, while the YB1-INPs treatment resulted in abundant aggregation of YB1-INPs in the tumor due to the live bacteria carrier targeting the tumor hypoxic regions. Furthermore, the YB1-INPs with laser-induced photothermal treatment (abbreviated as YB1-INPs (+)) resulted in a pronounced increase in the fluorescent signal at the tumor site within 24 h, and the intensity at the site increased throughout the remainder of the time course (Fig. 4A). At 72 h after injection, the tumors and major organs of the mice were collected to further investigate the distribution of YB1-INPs. As shown in Fig. S3, the YB1-INPs with laser irradiation exhibited a high degree of tumor accumulation.

We conducted 4',6-diamidino-2-phenylindole (DAPI) nuclear staining and UltraSensitive™ S-P Kit (mouse/rabbit) YB1 staining of tumor sections for the 72-h treated samples to explore whether bacteria entered the tumor. The INPs-treated mice demonstrated no bacterial

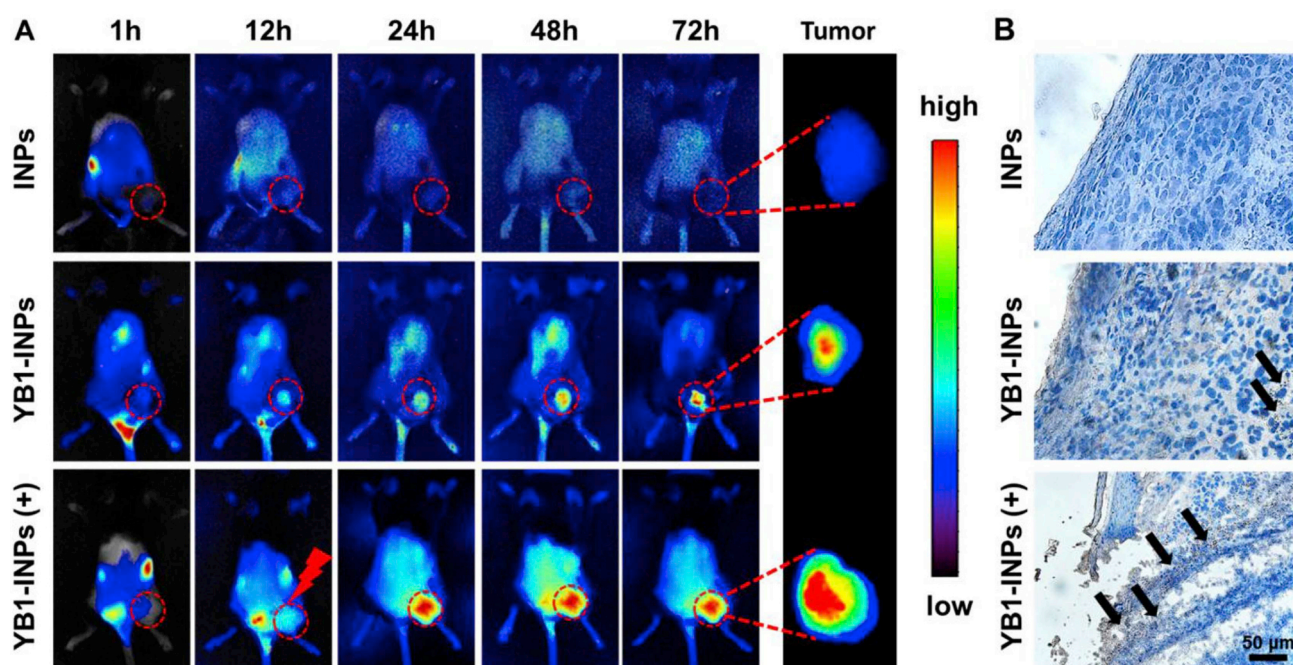


Fig. 4. *In vivo* photothermal-assisted bioaccumulation of YB1-INPs in large solid tumors. A) *In vivo* FL imaging of INPs, YB1-INPs and YB1-INPs (+) at different time points. (+) refers to laser irradiation at 12 h for promoting bioaccumulation of YB1-INPs. The *ex vivo* NIR FL images of tumors at 72 h. B) Immunohistochemistry images of tumor sections at 72 h. The results showed enhanced bioaccumulation of YB1-INPs in photothermal-disrupted tumors. The black dots indicated by arrows represent YB1-INPs colonies.

distribution in the tumor sections, while the YB1-INPs-treated mice exhibited apparent bacterial (black dots) accumulation. The YB1-INPs mice that received photothermal treatment had a vastly different appearance. There was obvious damage and loosening in the tumor, and a great deal of bacteria (black dots) were apparently aggregated in gaps along the surface (Fig. 4B). The results showed that perfect photothermal intervention of YB1-INPs could break through formidable physical barrier (dense packing of tumor cells and the fibrous tumor stroma) to promote bacterial diffusion in tumor.

The time curve of blood circulation was investigated by quantifying the ICG concentration at different time points after the intravenous injection of YB1-INPs or INPs to C57BL/6 mice (Fig. S4). ICG concentration in the blood when loaded to YB1 was significantly higher than that of INPs at the first 15 min after injection. The AUC_{24h} (the area under the plasma drug concentration-time curve over the period of 24 h) of YB1-INPs was $224 \mu\text{g min}\cdot\text{mL}^{-1}$, which was 3-fold higher than that of INPs ($69 \mu\text{g min}\cdot\text{mL}^{-1}$). These data indicated that YB1-INPs could significantly improve the drug bioavailability.

Meanwhile, we investigated the excretion pathway of YB1-INPs from the body. According to the reported method [40], we measured ICG content in urine and feces of C57BL/6 mice at 24 h post-injection. The excretion of urine ICG was $2.21 \pm 0.97 \mu\text{g}$, and fecal ICG excretion was $0.03 \pm 0.02 \mu\text{g}$ in 24 h, which suggested that ICG in INPs had the excretion pathways mainly from the liver into the small intestine and subsequently into fecal excretion. Moreover, neutrophils effectively kill *Salmonella*, primarily via production of lethal concentrations of ROS or hypochlorite (chlorox) in the phagosome [46,47]. YB1 were mainly cleared by neutrophils in mice, not by fecal and urine excretion [46,47].

3.4. Assessment of YB1-driven hypoxia-targeting and photothermal-assisted bioaccumulation in whole tumors

To better visualize the hypoxic tumor regions and to demonstrate colocalization of YB1, *ex vivo* immunofluorescence imaging of transverse tumor sections of the YB1-INP group were acquired using an Invitrogen EVOS FL Auto 2 system (Fig. 5A). Sections were stained with

anti-Salmonella antibody (YB1, purple), FITC-Mab1 (hypoxia, green), DAPI (DNA, blue), and ICG (INPs, red). The colocalization of YB1 and ICG revealed that conjugated YB1-INPs as a whole enter the large solid tumor after circulating in the blood (Fig. 5A, a₁, a₂). Transverse tumor section images and corresponding surface plot images demonstrated that YB1-INPs microswimmers with self-driven power can realize tumor accumulation by targeting hypoxia in the tumor cores (Fig. 5A, a₂, 5a₃, 5a₆, 5a₇ and 5C).

To explore the photothermal-assisted bioaccumulation efficiency of YB1-INPs, transverse tumor sections of the YB1-INPs (+) laser group were stained for immunofluorescence imaging (Fig. 5b₁-b₄), and the images were converted to surface plots (Fig. 5b₅-b₈). As shown in Fig. 5b₁, the large areas of the ICG FL signal indicated that the YB1-INPs were more extensively distributed throughout the large solid tumor after laser intervention. However, YB1-INPs were mainly localized in the tumor cores region in the absence of the laser irradiation (Fig. 5a₁, 5a₅).

To further test whether photothermal assistance at 12 h post-injection could effectively increase the accumulation of YB1-INPs for tumor penetrative therapy, the FL intensity at the arrows in Fig. 5a₁ and Fig. 5b₁ was measured by semiquantitative analysis (Fig. 5D). These integral results of the FL intensity indicated that INPs-mediated photothermal intervention for damaging the tumor tissue could significantly promote 14-fold more YB1-INPs to pass into the whole tumor, as shown by the result in Fig. S3b. The results indicated that the YB1-INPs penetrated into tumor hypoxic cores, and tissue damage induced by laser irradiation promoted the bioaccumulation of YB1-INPs in large solid tumors.

3.5. *In vivo* photothermal therapy of YB1-INPs enhanced by hypoxia-targeting and photothermal-assisted bioaccumulation

Next, we sought to evaluate the therapeutic effect of photothermal therapy paired with YB1-INPs for large solid tumors ($\geq 500 \text{ mm}^3$ in volume). The tumor regions were treated with the first dose of NIR laser irradiation (denoted as (+)) at 12 h after intravenous injection of YB1-INPs. The first dose of laser irradiation could kill tumor cells to produce

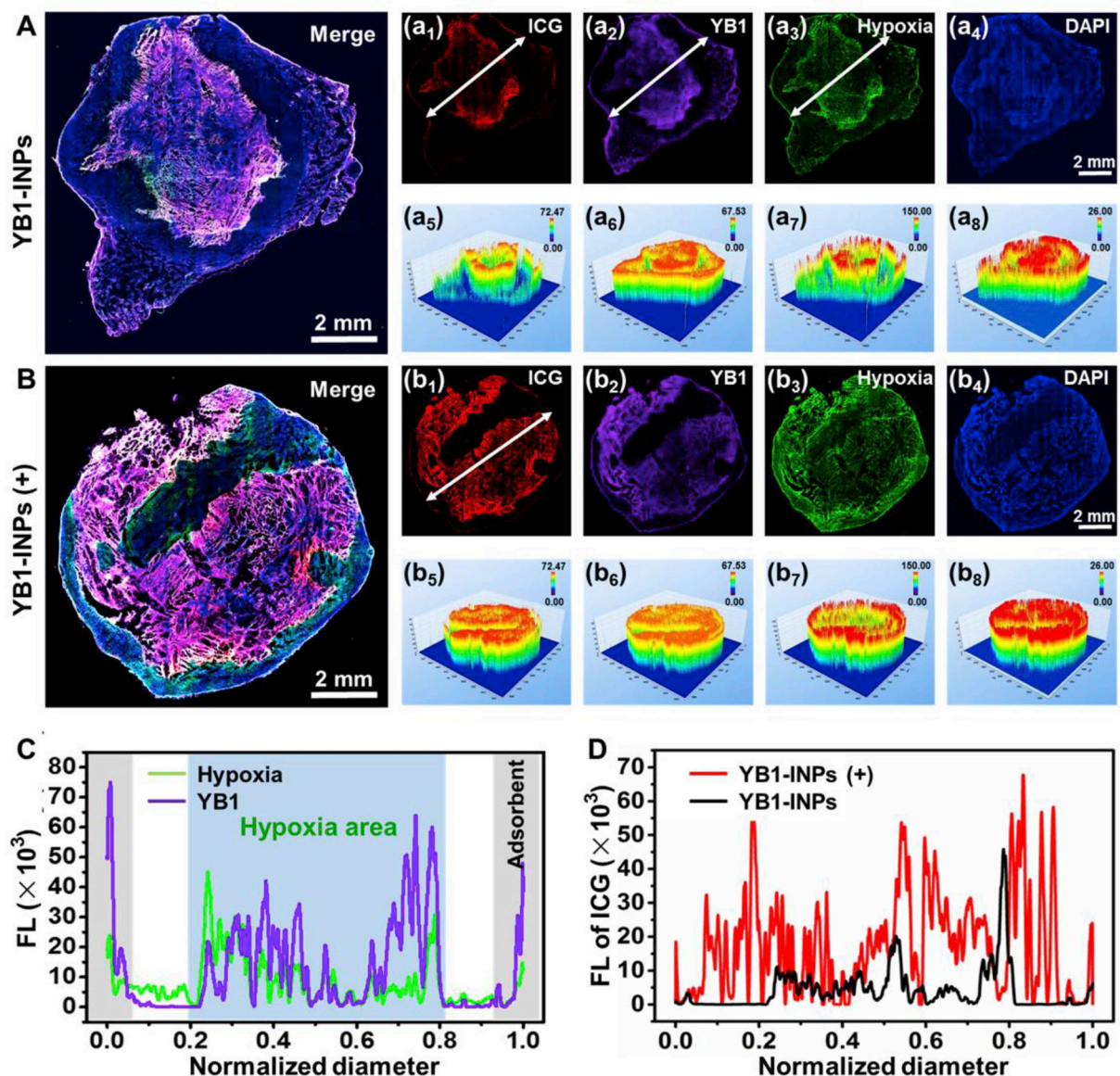


Fig. 5. Hypoxia targeting of YB1-INPs and photothermal-assisted bioaccumulation in large solid tumors. A, B) Immunofluorescence imaging of transverse tumor sections at 72 h. Sections were stained with anti-Salmonella antibody (YB1, purple), FITC-Mab1 (hypoxia, green), DAPI (DNA, blue), and ICG (INPs, red) (Fig. 5a₁-a₄, b₁-b₄). Surface plot images were analyzed with Celleste™ software (Fig. 5a₅-a₈, b₅-b₈). (+) refers to laser irradiation. C) FL intensity of the underlined part in Figure a₂ and a₃ indicates that YB1-INPs achieved tumor accumulation by targeting hypoxia in the tumor cores. D) ICG FL intensity of YB1-INPs (a₁) and YB1-INPs (+) (b₁) demonstrated that laser irradiation significantly enhanced YB1-INPs accumulation. (For interpretation of the references to color in this figure legend, the reader is referred to the Web version of this article.)

bacteria-attracting nutrients and further loosen the tumor tissue, resulting in the recruitment of more YB1-INPs and promoting YB1-INP infiltration. The second laser (denoted as + laser) was used to ablate the tumor on day 3 (Fig. 6A). As shown in Fig. 6B, the temperature increase in the tumor region after second laser irradiation was investigated on day 3. For the PBS (+) + laser or INPs (+) + laser groups, the temperature of tumors only increased to 40 or 42 °C, which was not high enough to destroy the tumors (43 °C causes irreversible tumor damage) (Fig. 6B) [35]. Due to YB1-driven hypoxia targeting and photothermal-assisted bioaccumulation, YB1-INPs induced a maximum temperature up to 63 °C, which successfully aided in killing tumor cells (Fig. 6B). It is worth noting that hyperthermia (63 °C) could also eliminate YB1 in the tumors to realize a safe and effective treatment (Fig. 5S).

As shown in Fig. 6D, MB49 tumors treated with PBS (+) + laser grew rapidly, illustrating that laser irradiation had no effect on tumor

growth (Fig. 5S6). There was also no apparent efficacy in restricting the growth of tumors in the INPs (+) + laser group due to the low tumor accumulation of INPs after intravenous injection and the first laser intervention (Fig. 6D and C). YB1-INPs could inhibit tumor growth, but tumor growth eventually recurred (Fig. 6D and C). Due to YB1-driven hypoxia targeting and photothermal-assisted bioaccumulation, YB1-INPs (+) + laser achieved a low dose and high efficiency photothermal therapy. The treatment dose of YB1-INPs (+) + laser was reduced to approximately one-fifth dose of already reported INPs [35]. Notably, the tumor inhibition rate of YB1-INPs (+) + laser was 100% at 28 days. And even more exciting the survival rate (YB1-INPs (+) + laser) was 100% at the end of the experiment (Fig. 6E). The tumor tissue damage after different treatment was evaluated at 3 days post-treatment (Fig. 6F). As expected, YB1-INPs (+) Laser group exhibited the highest level of cancer-cell damage, due to YB1 mediated anti-tumor effect and INPs induced thermal damage. The toxicity of YB1-INPs to

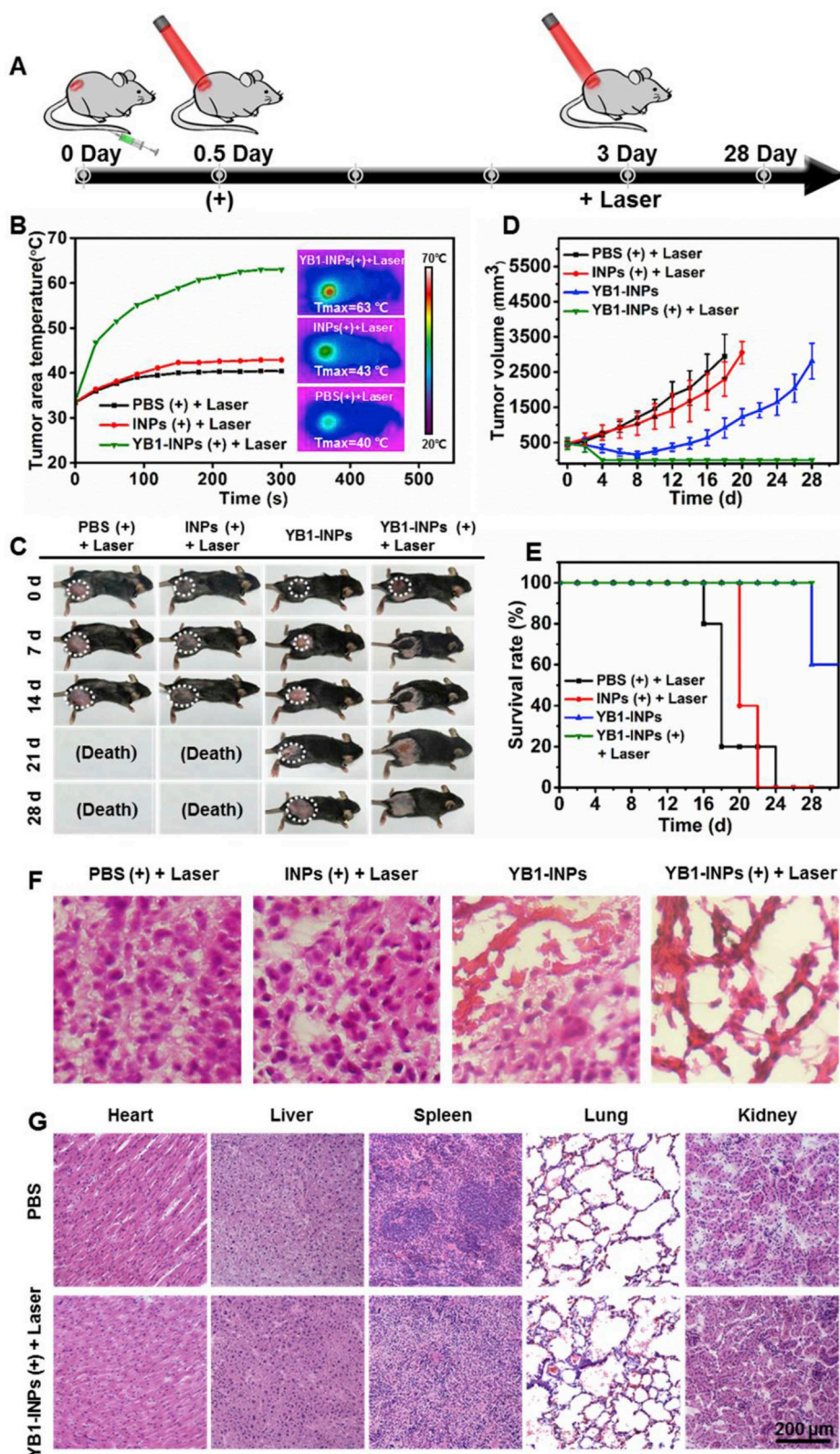


Fig. 6. *In vivo* YB1-INPs photothermal therapy of large solid tumors. A) Schematic diagram depicting the YB1-INPs treatment protocol for tumor eradication. B) Infrared thermal images of MB49 tumor-bearing mice exposed to laser irradiation after intravenous injection of PBS, INPs or YB1-INPs at 72 h. C) Representative photos of mice bearing MB49 tumors after treatment. D) Tumor growth curves after treatment (n = 5). YB1-INPs (+) + laser conferred a higher photothermal therapy effect and no tumor recurrence. E) Survival rates of mice (n = 5). F) H&E stained histological sections of the excised tumors 72 h after injection of PBS, INPs, and YB1-INPs under laser irradiation. G) H&E staining of the major organs of mice on day 28.

major organs was investigated by hematoxylin and eosin (H&E) staining and liver/kidney function indices (liver function indices: alanine aminotransferase (ALT), alkaline phosphatase (ALP); kidney function indices: creatinine (CREA) and UREA according to blood biochemistry tests (Figs. 6G and S8). As shown in Fig. 6G, H&E staining revealed that the distribution of neutrophils in the spleen of the YB1-INPs (+) + laser group differed from that of the control group because the

spleen is the main metabolic organ of bacteria. The histological morphology of other organs showed no obvious change compared with the control group. The body weights of the mice increased, suggesting that the YB1-INPs (+) + laser treatment was well tolerated by the mice (Fig. S7). The concentrations of ALT/ALP/CREA/UREA showed no obvious changes compared with the control group (Fig. S8). These results demonstrated that the YB1-INPs under laser excitation can offer

high-safety and high-efficiency photothermal therapy for large solid tumors.

4. Conclusion

We developed a biotic/abiotic hybrid system, YB1-INPs, to achieve high-efficiency tumor targeting and tumor elimination. By exploiting the inherent nature of YB1 strains, the use of self-motivated YB1 allowed us to overcome the shortcomings of classical nanoparticles in tumor targeting and penetration. Such a YB1-INPs bacteria-driven delivery strategy achieved highly selective hypoxia-targeting of delivering INPs, and most importantly, photothermal tumor lysis, as the bacteria-attracting nutrients also improved the accumulation of YB1-INPs. In addition, the YB1-INPs displayed excellent real-time FL imaging ability, which allowed us to more accurately monitor the tumor-targeting and tumor penetration of YB1-INPs. Benefiting from the mutual promotion of both YB1 and INPs, YB1 enabled the penetration of INPs deep into tumors; subsequently, the tumor regions temperature rose to 63 °C after NIR laser irradiation treatment, resulting in the simultaneous eradication both of intratumoral YB1 and the large solid tumor ($\geq 500 \text{ mm}^3$). The corresponding *in vitro* and *in vivo* results confirmed the unique advantages of YB1-INPs in tumor hypoxia-targeting and tumor tissue penetration. Overall, this bacteria-mediated hypoxia-targeting delivery strategy provides a new approach for combining theranostics nanotechnology with bacterial microswimmers to achieve superior anticancer effects.

Data availability statement

The raw/processed data required to reproduce these findings cannot be shared at this time as the data also forms part of an ongoing study.

Acknowledgment

The work was supported by the Key International S&T Cooperation Project (2015DFH50230), the National Natural Science Foundation of China (No. 31571013, 81701816, 81501591, 81671758, 21701033, 81501580, 91731302, and 51502333), Natural Science Foundation of Guangdong Province (2017A030313079, 2017A030313726 and 2016A030312006), Shenzhen Science and Technology Program (GJHS20140610152828690, JSGG20160331185422390, JCYJ2016042 9191503002, JCYJ20170818164139781), Shenzhen Peacock Team Project (KQTD2015033117210153), the key research program of the Chinese Academy of Sciences (KFZD-SW-216), SIAT Innovation Program for Excellent Young Researchers (Y7G005) and Dongguan Project on Social Science and Technology Development (2015108101019), the LU JIAXI International team programme supported by the K.C. Wong Education Foundation and CAS (GJTD-2018-14).

Appendix A. Supplementary data

Supplementary data to this article can be found online at <https://doi.org/10.1016/j.biomaterials.2019.119226>.

References

- [1] M.O. Din, T. Danino, A. Prindle, M. Skalak, J. Selimkhanov, K. Allen, E. Julio, E. Atolia, L.S. Tsimring, S.N. Bhatia, J. Hasty, Synchronized cycles of bacterial lysis for *in vivo* delivery, *Nature* 536 (2016) 81.
- [2] J.-X. Fan, Z.-H. Li, X.-H. Liu, D.-W. Zheng, Y. Chen, X.-Z. Zhang, Bacteria-mediated tumor therapy utilizing photothermally-controlled TNF- α expression via oral administration, *Nano Lett.* 18 (4) (2018) 2373–2380.
- [3] N.S. Forbes, Engineering the perfect (bacterial) cancer therapy, *Nat. Rev. Canc.* 10 (2010) 785.
- [4] D.-W. Zheng, Y. Chen, Z.-H. Li, L. Xu, C.-X. Li, B. Li, J.-X. Fan, S.-X. Cheng, X.-Z. Zhang, Optically-controlled bacterial metabolite for cancer therapy, *Nat. Commun.* 9 (1) (2018) 1680.
- [5] Z. Hosseinidoust, B. Mostaghaci, O. Yasa, B.-W. Park, A.V. Singh, M. Sitti, Bioengineered and biohybrid bacteria-based systems for drug delivery, *Adv. Drug Deliv. Rev.* 106 (2016) 27–44.
- [6] X. Cheng, X. Zhang, Y. Zhou, C. Zhang, Z.-C. Hua, A *Salmonella Typhimurium* mutant strain capable of RNAi delivery, *Cancer Biol. Ther.* 15 (8) (2014) 1068–1076.
- [7] K.B. Low, M. Ittensohn, T. Le, J. Platt, S. Sodi, M. Amoss, O. Ash, E. Carmichael, A. Chakraborty, J. Fischer, S.L. Lin, X. Luo, S.I. Miller, L.-m. Zheng, I. King, J.M. Pawelek, D. Bermudes*, Lipid A mutant *Salmonella* with suppressed virulence and TNF α induction retain tumor-targeting *in vivo*, *Nat. Biotechnol.* 17 (1999) 37.
- [8] R.M. Ryan, J. Green, P.J. Williams, S. Tazzyman, S. Hunt, J.H. Harmey, S.C. Kehoe, C.E. Lewis, Bacterial delivery of a novel cytotoxin to hypoxic areas of solid tumors, *Gene Ther.* 16 (2009) 329.
- [9] C.A. Swofford, N. Van Dessel, N.S. Forbes, Abstract 3538: quorum-sensing *Salmonella* selectively trigger protein expression within tumors, *Cancer Res.* 75 (15 Supplement) (2015) 3538.
- [10] K. Yazawa, M. Fujimori, J. Amano, Y. Kano, S.i. Taniguchi, *Bifidobacterium longum* as a delivery system for cancer gene therapy: selective localization and growth in hypoxic tumors, *Cancer Gene Ther.* 7 (2) (2000) 269–274.
- [11] P. Lambin, J. Theys, W. Landuyt, P. Rijken, A. van der Kogel, E. van der Schueren, R. Hodgkiss, J. Fowler, S. Nuyts, E. de Bruijn, L. Van Mellaert, J. Anné, Colonization of *Clostridium* in the body is restricted to hypoxic and necrotic areas of tumours, *Anaerobe* 4 (4) (1998) 183–188.
- [12] L.H. Dang, C. Bettgowda, D.L. Huso, K.W. Kinzler, B. Vogelstein, Combination bacteriolytic therapy for the treatment of experimental tumors, *Proc. Natl. Acad. Sci. Unit. States Am.* 98 (26) (2001) 15155.
- [13] B. Yu, M. Yang, L. Shi, Y. Yao, Q. Jiang, X. Li, L.-H. Tang, B.-J. Zheng, K.-Y. Yuen, D.K. Smith, E. Song, J.-D. Huang, Explicit hypoxia targeting with tumor suppression by creating an “obligate” anaerobic *Salmonella Typhimurium* strain, *Sci. Rep.* 2 (2012) 436.
- [14] R.W. Kasinskas, N.S. Forbes, *Salmonella Typhimurium* specifically chemotax and proliferate in heterogeneous tumor tissue *in vitro*, *Biotechnol. Bioeng.* 94 (4) (2006) 710–721.
- [15] R.W. Kasinskas, N.S. Forbes, *Salmonella Typhimurium* lacking ribose chemoreceptors localize in tumor quiescence and induce apoptosis, *Cancer Res.* 67 (7) (2007) 3201.
- [16] B.-T. Ning, B. Yu, S. Chan, J.-I. Chan, J.-D. Huang, G.C.-F. Chan, Treatment of neuroblastoma with an engineered “obligate” anaerobic *Salmonella typhimurium* strain YB1, *J. Cancer* 8 (9) (2017) 1609–1618.
- [17] C.-H. Lee, C.-L. Wu, S.-H. Chen, A.-L. Shiau, Humoral immune responses inhibit the antitumor activities mediated by *Salmonella enterica* serovar choleraesuis, *J. Immunother.* 32 (4) (2009) 376–388.
- [18] F.J. Burrows, P.E. Thorpe, Eradication of large solid tumors in mice with an immunotoxin directed against tumor vasculature, *Proc. Natl. Acad. Sci. Unit. States Am.* 90 (19) (1993) 8996–9000.
- [19] R.B. Liu, B. Engels, A. Arina, K. Schreiber, E. Hyjek, A. Schietinger, D.C. Binder, E. Butz, T. Krausz, D.A. Rowley, B. Jabri, H. Schreiber, Densely Granulated Murine NK Cells Eradicate Large Solid Tumors, *Cancer Research*, 2012 canres.3208.2011.
- [20] N. Agrawal, C. Bettgowda, I. Cheong, J.-F. Geschwind, C.G. Drake, E.L. Hipkiss, M. Tatsumi, L.H. Dang, L.A. Diaz, M. Pomper, M. Abusedera, R.L. Wahl, K.W. Kinzler, S. Zhou, D.L. Huso, B. Vogelstein, Bacteriolytic therapy can generate a potent immune response against experimental tumors, *Proc. Natl. Acad. Sci. U. S. A.* 101 (42) (2004) 15172–15177.
- [21] I. Cheong, X. Huang, C. Bettgowda, L.A. Diaz, K.W. Kinzler, S. Zhou, B. Vogelstein, A bacterial protein enhances the release and efficacy of liposomal cancer drugs, *Science* 314 (5803) (2006) 1308–1311.
- [22] C. Qian, P. Feng, J. Yu, Y. Chen, Q. Hu, W. Sun, X. Xiao, X. Hu, A. Bellotti, Q.-D. Shen, Z. Gu, Anaerobe-inspired anticancer nanovesicles, *Angew. Chem. Int. Ed.* 56 (10) (2017) 2588–2593.
- [23] L. Tang, Y. Zheng, M.B. Melo, L. Mabardi, A.P. Castaño, Y.-Q. Xie, N. Li, S.B. Kudchodkar, H.C. Wong, E.K. Jeng, M.V. Maus, D.J. Irvine, Enhancing T cell therapy through TCR-signaling-responsive nanoparticle drug delivery, *Nat. Biotechnol.* 36 (2018) 707.
- [24] C.-H. Luo, C.-T. Huang, C.-H. Su, C.-S. Yeh, Bacteria-mediated hypoxia-specific delivery of nanoparticles for tumors imaging and therapy, *Nano Lett.* 16 (6) (2016) 3493–3499.
- [25] O. Felfoul, M. Mohammadi, S. Taherkhani, D. de Lanauze, Y. Zhong Xu, D. Loghini, S. Essa, S. Jancic, D. Houle, M. Lafleur, L. Gaboury, M. Tabrizian, N. Kaou, M. Atkin, T. Vuong, G. Batist, N. Beauchemin, D. Radzioch, S. Martel, Magneto-aerotactic bacteria deliver drug-containing nanoliposomes to tumour hypoxic regions, *Nat. Nanotechnol.* 11 (2016) 941.
- [26] J. Xue, Z. Zhao, L. Zhang, L. Xue, S. Shen, Y. Wen, Z. Wei, L. Wang, L. Kong, H. Sun, Q. Ping, R. Mo, C. Zhang, Neutrophil-mediated anticancer drug delivery for suppression of postoperative malignant glioma recurrence, *Nat. Nanotechnol.* 12 (2017) 692.
- [27] S. Shen, Y. Chao, Z. Dong, G. Wang, X. Yi, G. Song, K. Yang, Z. Liu, L. Cheng, Bottom-up preparation of uniform ultrathin rhenium disulfide nanosheets for image-guided photothermal radiotherapy, *Adv. Funct. Mater.* 27 (28) (2017) 1700250.
- [28] J. Wang, Y. Li, L. Deng, N. Wei, Y. Weng, S. Dong, D. Qi, J. Qiu, X. Chen, T. Wu, High-performance photothermal conversion of narrow-bandgap Ti2O3 nanoparticles, *Adv. Mater.* 29 (3) (2016) 1603730.
- [29] J. Shao, H. Xie, H. Huang, Z. Li, Z. Sun, Y. Xu, Q. Xia, X.-F. Yu, Y. Zhao, H. Zhang, H. Wang, P.K. Chu, Biodegradable black phosphorus-based nanospheres for *in vivo* photothermal cancer therapy, *Nat. Commun.* 7 (2016) 12967.
- [30] D. Wang, H. Wu, J. Zhou, P. Xu, C. Wang, R. Shi, H. Wang, H. Wang, Z. Guo, Q. Chen, *In situ* one-pot synthesis of MOF-polydopamine hybrid nanogels with

- enhanced photothermal effect for targeted cancer therapy, *Advanced Science* 5 (6) (2018) 1800287.
- [31] H. Zhang, Q. Li, R. Liu, X. Zhang, Z. Li, Y. Luan, A versatile prodrug strategy to in situ encapsulate drugs in MOF nanocarriers: a case of cytarabine-IR820 prodrug encapsulated ZIF-8 toward chemo-photothermal therapy, *Adv. Funct. Mater.* 28 (35) (2018) 1802830.
- [32] X. Zhu, W. Feng, J. Chang, Y.-W. Tan, J. Li, M. Chen, Y. Sun, F. Li, Temperature-feedback upconversion nanocomposite for accurate photothermal therapy at facile temperature, *Nat. Commun.* 7 (2016) 10437.
- [33] Y. Liu, Q. Guo, X. Zhu, W. Feng, L. Wang, L. Ma, G. Zhang, J. Zhou, F. Li, Optimization of prussian blue coated NaDyF₄:x%Lu nanocomposites for multi-functional imaging-guided photothermal therapy, *Adv. Funct. Mater.* 26 (28) (2016) 5120–5130.
- [34] Y. Liu, Q. Jia, Q. Guo, W. Wei, J. Zhou, Simultaneously activating highly selective ratiometric MRI and synergistic therapy in response to intratumoral oxidability and acidity, *Biomaterials* 180 (2018) 104–116.
- [35] Z. Chen, P. Zhao, Z. Luo, M. Zheng, H. Tian, P. Gong, G. Gao, H. Pan, L. Liu, A. Ma, H. Cui, Y. Ma, L. Cai, Cancer cell membrane-biomimetic nanoparticles for homologous-targeting dual-modal imaging and photothermal therapy, *ACS Nano* 10 (11) (2016) 10049–10057.
- [36] M. Zheng, C. Yue, Y. Ma, P. Gong, P. Zhao, C. Zheng, Z. Sheng, P. Zhang, Z. Wang, L. Cai, Single-step assembly of DOX/ICG loaded lipid-polymer nanoparticles for highly effective chemo-photothermal combination therapy, *ACS Nano* 7 (3) (2013) 2056–2067.
- [37] S. Taherkhani, M. Mohammadi, J. Daoud, S. Martel, M. Tabrizian, Covalent binding of nanoliposomes to the surface of magnetotactic bacteria for the synthesis of self-propelled therapeutic agents, *ACS Nano* 8 (5) (2014) 5049–5060.
- [38] Q. Hu, M. Wu, C. Fang, C. Cheng, M. Zhao, W. Fang, P.K. Chu, Y. Ping, G. Tang, Engineering nanoparticle-coated bacteria as oral DNA vaccines for cancer immunotherapy, *Nano Lett.* 15 (4) (2015) 2732–2739.
- [39] T.H. Segall-Shapiro, E.D. Sontag, C.A. Voigt, Engineered promoters enable constant gene expression at any copy number in bacteria, *Nat. Biotechnol.* 36 (2018) 352.
- [40] V. Saxena, M. Sadoqi, J. Shao, Polymeric nanoparticulate delivery system for Indocyanine green: biodistribution in healthy mice, *Int. J. Pharm.* 308 (1) (2006) 200–204.
- [41] H. Tian, Z. Luo, L. Liu, M. Zheng, Z. Chen, A. Ma, R. Liang, Z. Han, C. Lu, L. Cai, Cancer cell membrane-biomimetic oxygen nanocarrier for breaking hypoxia-induced chemoresistance, *Adv. Funct. Mater.* 27 (38) (2017) 1703197.
- [42] Y. Wang, Y. Xie, J. Li, Z.-H. Peng, Y. Sheinin, J. Zhou, D. Oupický, Tumor-penetrating nanoparticles for enhanced anticancer activity of combined photodynamic and hypoxia-activated therapy, *ACS Nano* 11 (2) (2017) 2227–2238.
- [43] T. Ahmad, M. Gogarty, E.G. Walsh, D.J. Brayden, A comparison of three Peyer's patch "M-like" cell culture models: particle uptake, bacterial interaction, and epithelial histology, *Eur. J. Pharm. Biopharm.* 119 (2017) 426–436.
- [44] Y. Alapan, O. Yasa, O. Schauer, J. Giltinan, A.F. Tabak, V. Sourjik, M. Sitti, Soft erythrocyte-based bacterial microswimmers for cargo delivery, *Science Robotics* 3 (17) (2018) eaar4423.
- [45] W. Chen, Y. Wang, M. Qin, X. Zhang, Z. Zhang, X. Sun, Z. Gu, Bacteria-driven hypoxia targeting for combined biotherapy and photothermal therapy, *ACS Nano* 12 (6) (2018) 5995–6005.
- [46] J.W. Conlan, Critical roles of neutrophils in host defense against experimental systemic infections of mice by *Listeria monocytogenes*, *Salmonella Typhimurium*, and *Yersinia enterocolitica*, *Infect. Immun.* 65 (2) (1997) 630.
- [47] S. Eriksson, S. Lucchini, A. Thompson, M. Rhen, J.C.D. Hinton, Unravelling the biology of macrophage infection by gene expression profiling of intracellular *Salmonella enterica*, *Mol. Microbiol.* 47 (1) (2003) 103–118.